Available online at www.sciencedirect.com

ScienceDirect

Procedia Structural Integrity 38 (2022) 604–610

Structural Integrity Procedia

www.elsevier.com/locate/procedia

FATIGUE DESIGN 2021, 9th Edition of the International Conference on Fatigue Design

Designing very high-cycle fatigue specimens of additively manufactured Ti-6Al-4V with different porosities and microstructures

Grégoire Brot[a,b]*, Véronique Favier[b], Imade Koutiri[b], Vincent Bonnand[a], Corinne Dupuy[b], Nicolas Ranc[b], Fabien Lefebvre[c]

[a]*DMAS, ONERA, Université Paris Saclay, F-92322 Châtillon - France*
[b]*PIMM, Arts et Metiers Institute of Technology, CNRS, Cnam, HESAM University, 151 Boulevard de l'Hopital, Paris (France)*
[c]*CETIM, 60304 Senlis, France*

Abstract

High cycle fatigue properties of material obtained with additive manufacturing (AM) processes such as LPBF (Laser Powder Bed Fusion) remain misunderstood. These properties are complex due to the porous and anisotropic features of AM parts. Moreover, a high number of process parameters can influence the obtained fatigue behavior. In this context, a rapid determination of the high and very high cycle fatigue properties is necessary in order to optimize process parameters with regard to fatigue response. This first work aims to produce test pieces with different porosity rates and microstructures. The processing and post-processing parameters leading to different porosity rates, porosity size distribution and microstructure are determined and presented. In a future work, the fatigue response will be then compare using two accelerated fatigue determination methods: ultrasonic fatigue testing and fatigue limit evaluation through lock-in thermography.

Keywords: Additive manufacturing, Very-high-cycle fatigue, Ti-6Al-4V, Porosity

* Corresponding author.
E-mail address: gregoire.brot@ensam.eu

10.1016/j.prostr.2022.03.062

1. Introduction

Thanks to the rapid development of metallic additive manufacturing (AM) technics, Ti-6Al-4V parts produced with LPBF (Laser Powder Bed Fusion) show now mechanical properties that are comparable to the ones of conventionally manufactured ones. AM parts made of Ti-6Al-4V are more brittle than conventionally manufactured parts but reach higher yield and ultimate tensile stresses (Vrancken et al., 2012; Agius et al., 2018). Moreover, after an annealing treatment, the monotonic properties of AM Ti-6Al-4V get close to the ones of conventionally manufactured one. These suitable properties should be linked with the relatively low porosity rate of Ti-6Al-4V pieces produced with LPBF process. Porosity rates lower than 0.5 % can be obtained without specific difficulty (Thijs et al., 2010; Kasperovich and Hausmann, 2015; Kumar et al., 2018). Nevertheless, these relatively low porosity rates are of course a major issue due to the high sensitivity of fatigue behavior to defect. Indeed, LPBF and other AM processes are cost-intensive processes (Rickenbacher et al., 2013), which can economically be used only for strong value-added pieces, that are also often fatigue-loaded parts. As a result, research focusses on few alloy such as Ti-6Al-4V and especially their fatigue behaviors. Moreover, these materials are often used in transportation industries, in which the fatigue lifespan of pieces can reach 10^{10} cycles (Bathias and Paris, 2005). The resistance of these materials in the very high cycle fatigue (VHCF) regime, beyond 10^7 cycles, is therefore of a great interest. Fatigue behaviors of LPBF parts are complex as they show anisotropic properties and contain pores which act as fatigue crack initiation sites. Furthermore, LPBF process comes with a high number of process parameters (Spears and Gold, 2016) and many of them can influence the fatigue behavior. In this context, a rapid determination of the high and very high cycle fatigue (VHCF) properties is necessary in order to optimize process parameters with regard to fatigue response.

The most widely used approach to study VHCF is the ultrasonic fatigue testing method. This technic consists in a high frequency fatigue test during which test samples are being held in a free resonance mode. The high testing frequency, often close to 20 kHz, allows studying lifespan up to 10^9 cycles within a day. However, Papakyriacou et al. and other authors have shown that the fatigue testing frequency can have an effect on the fatigue behavior (Papakyriacou et al., 2001). In some case, ultrasonic fatigue results cannot be directly used to design industrial parts submitted to lower fatigue frequency. Fatigue limit assessment through infrared (IR) thermography is another possibility to examine VHCF behavior. This method examines the self-heating behavior of sample submitted to cyclic loading with different stress amplitudes. Under low stresses, self-heating of the sample is mainly due to irreversible but recoverable deformation, called anelastic dissipation mechanisms (Mareau et al., 2012). Beyond a threshold stress amplitude, when local plasticity causes enough dissipations, a new self-heating regime appears. Supposing that this local plasticity is enough to lead to a finite lifespan, the threshold stress amplitude is hence an estimation of the fatigue limit. In order to shorten testing time, Krapez et al. first applied this method using lock-in thermography measuring technics (Krapez et al., 2000). Indeed, they measured the self-heating during a few tens of cycles for each stress level.

Even if the fatigue properties of additively manufactured Ti-6Al-4V remains misunderstood, some trends emerge. Surface treatments appear to have the greatest effect on fatigue strength (Li et al., 2016; Bagehorn et al., 2017), then comes the effect of thermal post-treatments. In order to achieve acceptable fatigue properties, LPBF parts should be post-processed. Indeed, the fatigue strength at 10^6 cycles of as build LPBF Ti-6Al-4V is between 70 and 300 MPa (Wycisk et al., 2013; Edwards and Ramulu, 2014; Bagehorn et al., 2017), whereas this strength for LPBF part that are both machined and heat treated is over 400 MPa (Leuders et al., 2013; Rafi et al., 2013; Wycisk et al., 2013, 2014). The highest fatigue strength is reached for specimens that are treated with a hot isostatic pressing (HIP) process and then machined. Leuders et al. obtained a fatigue strength at 10^6 cycles of 630 MPa on specimens that were HIPed at 920°C for 2 h under 100 MPa (Leuders et al., 2013).

Moreover, fatigue samples of Ti-6Al-4V produced with LPBF show a high scatter and relatively a limited anisotropy of their fatigue properties (Chastand et al., 2018; Le et al., 2019). Le et al. showed this anisotropy on specimens printed at 0°, 45° or 90° to the building direction. This anisotropy is mainly due to the anisotropic shape of pores, which tend to be larger in plan perpendicular to the building direction. Indeed, mapping approach that links the stress, the pore size and the fatigue life did not discriminate specimens with different building orientation (Le et al., 2019). Le et al. also concluded that the high scatter of fatigue results arises from the different types of fatigue crack initiation sites corresponding to different types of pores. This is also confirmed by the limited scatter of HIPed

specimens which are almost fully dense (Greitemeier et al., 2017). Moreover, fatigue crack does not necessarily initiate at the largest pore. Other parameters such as the position of the shape of pore affect the initiation. The most critical defect are surface lack of fusion followed by internal lack of fusion, surface gas pore and internal gas pore (Le et al., 2019). However, the influence of defect, such as pores, and microstructure on the fatigue behavior is still not fully understood. A high number of articles examined the high cycle fatigue (HCF) behavior of LPBF Ti-6Al-4V, whereas very few experimental campaigns were performed on its behavior in the VHCF domain. Wycisk et al. (Wycisk et al., 2015) and Günther et al. (Günther et al., 2017) both studied the tension-compression behavior of LPBF Ti-6Al-4V in the HCF and VHCF regimes. Both campaigns were performed using low frequency fatigue in the high cycle regime and ultrasonic fatigue in the very high cycle regime. None of the authors reported a clear effect of the loading frequency on the fatigue strength. Nevertheless, conclusion on this effect cannot be drawn, as the lifespan domains, studied with each fatigue technic, did not recover themselves a lot in both articles. More recently, Du et al. (Du et al., 2021), examined VHCF response of LPBF Ti-6Al-4V under two load ratios. These three studies (Wycisk et al., 2015; Günther et al., 2017; Du et al., 2021), noticed a transition from surface to internal crack initiation around 10^7 cycles.

This work aims to obtain test pieces with five different grades of LPBF Ti-6Al-4V in order to examine the influence of microstructure and porosity on its very-high-cycle fatigue behavior. Three of them should have the same porosity but different microstructures and three of them should have different porosities with a similar microstructure.

2. Materials and methods

All test samples are printed using LaserForm® Ti Gr5 (A) powder from 3D Systems. LPBF processing is conducted with a SLM 125 machine from SLM Solutions. All test samples are fabricated vertically, their main axis corresponding to the build direction. Build platform is preheated at 150°C in order to limit residual stresses. During each fabrication batch, the ratio between the printed horizontal surface and the build platform surface is about 15 % in order to limit gas pollution in the build chamber. LPBF manufacturing parameters were chosen during an initial study. This study determined two sets of parameters leading to two different porosity rates, P_1 close to 0.05 % and P_2 close to 1 %. P_1 set correspond to parameters optimized to get the highest part density. The two sets of manufacturing parameters only differ by their laser scanning strategies. Main LPBF parameters are presented in Table 1. For both sets, skywriting function is being cut off during the fabrication; hence, the laser velocity is lower than the set point at each extremity of each laser track. At these locations, a higher energy density is brought by the laser, leading to likelier keyhole-porosity formation. When using the P_2 set, in which a chessboard scanning with an interlayer rotation of 15° is used, keyhole-porosities are created in a quasi-homogeneous way in the core of samples. On the contrary, no keyhole-porosities are formed in the core of parts fabricated with P_1 set. With both sets, keyhole-porosities are found in samples at about 200 µm from vertical edges (i.e. parallel to the building direction). These subsurface porosities are removed during post processing steps (i.e. machining or grinding). The two mentioned porosity rates correspond to the ones of the core of as-build parts.

Porosity of samples is evaluated using the micrographic cross section method. After cutting and polishing, samples are observed using optical microscopy. Porosity is assessed in horizontal plan (i.e. perpendicular to building direction). For each plan studied, 20 pictures with an x200 magnification are taken. Although there is no mutual agreement on criteria evaluating the impact of defect of fatigue life, all proposed criterion take into account the size of defect. Other parameters such as location or the shape of pores are also influencing fatigue life. The porosity rate in a sample is therefore not enough to characterize a population of pores in the fatigue context. The populations of pores in P_1 and P_2 samples are describe using the size and the circularity of pores. The size is determined as the square root of the measured area in accordance with Murakami's criteria. During micrographic image processing, only pores that are larger than 9 pixels (i.e. 0.9 µm²) are considered in order to avoid bad circularity assessment This measurement and the influence of measurement parameters such as the magnification or the number of picture have been deeply investigated by de Terris et al. (de Terris et al., 2019). Porosity evaluation is performed on at least three samples per set of parameter in order to asset the repeatability of the porosity of parts.

Table 1. LPBF manufacturing parameters used.

Manufacturing parameters	Laser power (W)	Scan velocity (mm/s)	Hatch distance (µm)	Layer thickness (µm)	Scanning strategy
P_1 set	275	1100	120	30	Stripes, no skywriting, interlayer rotation of 15°
P_2 set	275	1100	120	30	3 mm width chessboard, interlayer rotation of 15°

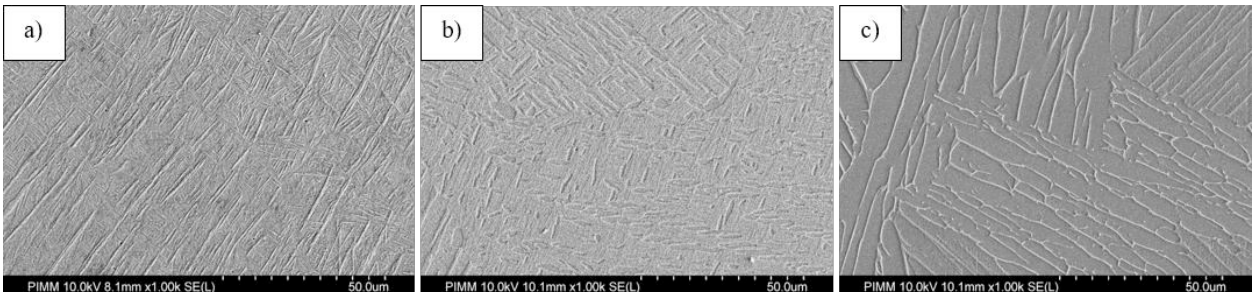

Fig 1. Etched surface of LPBF Ti-6Al-4V (a) As built. (b) After 2 h at 920°C, water-cooled. (c) After 2 h at 1020°C, air-cooled.

Thermal post-processing are used to get the five different material types that have different porosity rates (P_0, P_1, P_2) or microstructures (Fig 2). Three different thermal treatments are applied on as-build parts with a porosity P1, leading to three different microstructures with the same porosity. In as-build parts, the microstructure consists in lamellae of martensitic phase α' which results of the rapid cooling during LPBF process (Thijs et al., 2010). These lamellae, presented in Fig 1.a, are about 1 µm thick. As explain by Yang et al., α'-lamellae followed a hierarchical pattern explained by the intrinsic thermal treatments occurring during LPBF process (Yang et al., 2016).

The first treatment applied on as-build P_1 samples is a 3 hours long treatment at 650°C that releases residual stresses. This treatment does not change the morphology of the as-build microstructure, which is still an ultrafine lamellar one. However, the martensitic phase α' is fully decomposed into the thermodynamically stable phases α and β, according to the results of Gil Mur et al. (Gil Mur et al., 1996). The microstructure is therefore composed of α-lamellae surrounded by a very thin layer of β-phase (Lütjering and Williams, 2007). The second treatment consist of a sub β-transus treatment of 2 h at 920°C followed by a furnace cooling. This treatment cause the coarsening of α and β-lamellae and the spheroidisation of some α-grain, leading to a lamellar microstructure Fig 1.b. This microstructure is obtained for three different material grades that have different porosity rates. To do so, the treatment at 920°C is applied on as-build part with P_1 and P_2 porosity. Moreover, Leuders et al. showed that an HIP treatment of 2 hours at 920°C under 100 MPa closed most of the pores and lead to a nearly fully dense material (Leuders et al., 2013). The same HIP treatment, leading to a lamellar microstructure, is applied on as-build part with a P_1 porosity. The obtained porosity, almost null, is called P_0. The third microstructure with a P_1 porosity is obtained after a super-β-transus treatment at 1020°C for 2 h followed by a furnace cooling. It is composed of coarse α-grains surrounded by a thin layer of β phase visible in Fig 1.c (Vrancken et al., 2012). The strategy used to obtain the five grades is presented in Fig 2.

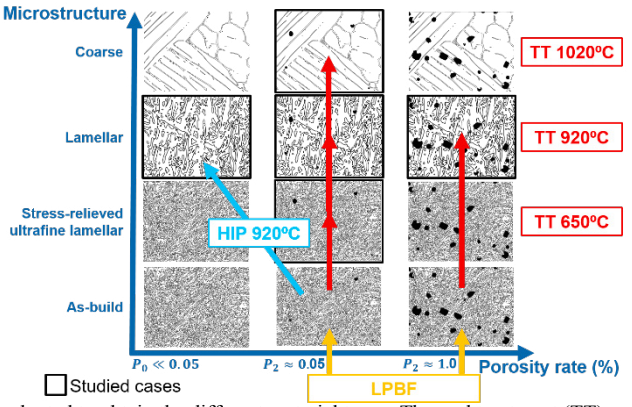

Fig 2. Strategy adopted to obtain the different material types. Thermal treatment (TT) and hot isostatic pressing (HIP) made using argon gas. HIP under 100 MPa. Adapted from (Vrancken et al., 2012).

The different processing routes used to obtain the five material grades are all applied on both test samples types presented in Fig 3. Ultrasonic test specimens are design so that the frequency of their first longitudinal resonating mode is equal to the one of the anti-resonance of the testing bench, which is close to 20 kHz. These parts are machined out of LPBF cylinders. Surface roughness of flat samples used for self-heating measurement is not crucial as no fatigue crack initiation is expected due to the low number of cycle performed. Therefore, the two main faces of these samples are grinded in order to avoid problems during IR thermography measurement.

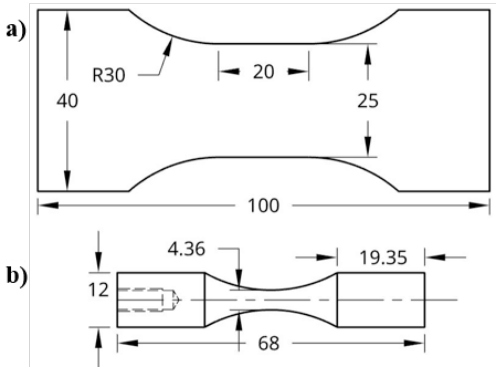

Fig 3. Geometries of the test samples: (a) 3 mm thick flat sample used for fatigue limit assessment through lock-in thermography and (b) sample used for ultrasonic fatigue test.

3. Results:

Comparison of P_1 and P_2 populations of defect obtained after LPBF processing is presented in Fig 4. In order to highlight the differences in terms of large defect size, Gumbel's reduced variable is determined for both populations. It should be noted that each point in Fig 4 correspond to an observed pore. The flatter the curve of the reduced variable is, the more pore with large size there are. The reduced variable Y is calculated from the cumulative distribution function F using equation (1).

$$Y = -\ln(-\ln(F)) \tag{1}$$

Gumbel's reduced variable for both populations show a linear tendency for large pores, meaning that these populations can be represented using Gumbel's law. The curves plotted in Fig 4.a correspond to the linear regression for all pores larger than 3 µm. In, terms of surface density of pores, there are 0.17 pores/mm² larger than 10 µm for P_1 population and 4.25/mm² pores larger than 10 µm for P_2 population. The relation between the size and the circularity of pores in presented in Fig 4.b. For pores smaller than 20 µm, there is no relation between size and circularity, whereas larger pores tend to be more circular. This is explained by the fact that large pores are mainly keyhole ones. For some small pores, which are captured by a small number of pixels, calculated circularity is slightly larger than one.

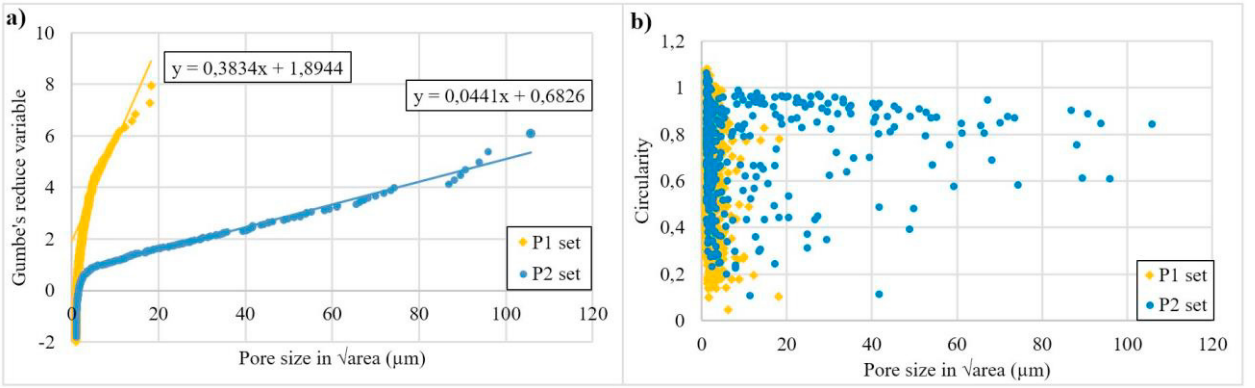

Fig 4. Comparison of P_1 and P_2 populations of defect. (a) Gumbel's reduced variable applied to the distribution of pore size. (b) Relation between size and circularity of pores

4. Conclusion

This work presented the processing and post-processing parameters of fatigue samples with different microstructures and pore populations. Following this first work, these samples will be examined with ultrasonic fatigue testing and fatigue limit assessment through lock-in thermography.

The main objective of the coming study is to compare and analyze the validity of both accelerated fatigue characterization methods. To the best of our knowledge, these methods were never both applied during a common campaign. This project aims to analyze the effect of both porosity and microstructure on the very high cycle fatigue behavior of Ti-6Al-4V manufactured with LPBF process. Another objective is to examine the possible influence of microstructure and porosity on the two accelerated methods. To do so, the five grades of test pieces obtained in this study will be tested with each accelerated testing method.

Acknowledgements

This work is made possible with the support of the consortium Additive Factory Hub, AFH.

References

Agius D, Kourousis KI, Wallbrink C (2018) A Review of the As-Built SLM Ti-6Al-4V Mechanical Properties towards Achieving Fatigue Resistant Designs. Metals 8(1): 75.

Bagehorn S, Wehr J, Maier HJ (2017) Application of mechanical surface finishing processes for roughness reduction and fatigue improvement of additively manufactured Ti-6Al-4V parts. International Journal of Fatigue 102: 135–142.

Bathias C, Paris PC (2005) Gigacycle Fatigue in Mechanical Practice. Marcel Dekker, New York.

Chastand V, Quaegebeur P, Maia W, Charkaluk E (2018) Comparative study of fatigue properties of Ti-6Al-4V specimens built by electron beam melting (EBM) and selective laser melting (SLM). Materials Characterization 143: 76–81.

Du L, Pan X, Qian G, Zheng L, Hong Y (2021) Crack initiation mechanisms under two stress ratios up to very-high-cycle fatigue regime for a selective laser melted Ti-6Al-4V. International Journal of Fatigue 149: 106294.

Edwards P, Ramulu M (2014) Fatigue performance evaluation of selective laser melted Ti–6Al–4V. Materials Science and Engineering: A 598: 327–337.

Gil Mur FX, Rodríguez D, Planell JA (1996) Influence of tempering temperature and time on the alpha'-Ti-6Al-4V martensite. Journal of Alloys and Compounds 234(2): 287–289.

Greitemeier D, Palm F, Syassen F, Melz T (2017) Fatigue performance of additive manufactured TiAl6V4 using electron and laser beam melting. International Journal of Fatigue 94: 211–217.

Günther J, Krewerth D, Lippmann T, Leuders S, Tröster T, Weidner A, Biermann H, Niendorf T (2017) Fatigue life of additively manufactured Ti–6Al–4V in the very high cycle fatigue regime. International Journal of Fatigue 94: 236–245.

Kasperovich G, Hausmann J (2015) Improvement of fatigue resistance and ductility of TiAl6V4 processed by selective laser melting. Journal of Materials Processing Technology 220: 202–214.

Krapez J-C, Pacou D, Gardette G (2000) Lock-in thermography and fatigue limit of metals. In: 2000 Quantitative InfraRed Thermography,.

Kumar P, Prakash O, Ramamurty U (2018) Micro-and meso-structures and their influence on mechanical properties of selectively laser melted Ti-6Al-4V. Acta Materialia 154: 246–260.

Le V-D, Pessard E, Morel F, Edy F (2019) Interpretation of the fatigue anisotropy of additively manufactured TA6V alloys via a fracture mechanics approach. Engineering Fracture Mechanics 214: 410–426.

Leuders S, Thöne M, Riemer A, Niendorf T, Tröster T, Richard HA, Maier HJ (2013) On the mechanical behaviour of titanium alloy TiAl6V4 manufactured by selective laser melting: Fatigue resistance and crack growth performance. International Journal of Fatigue 48: 300–307.

Li P, Warner DH, Fatemi A, Phan N (2016) Critical assessment of the fatigue performance of additively manufactured Ti–6Al–4V and perspective for future research. International Journal of Fatigue 85: 130–143.

Lütjering G, Williams JC (2007) Titanium. Springer, Berlin; New York.

Mareau C, Favier V, Weber B, Galtier A, Berveiller M (2012) Micromechanical modeling of the interactions between the microstructure and the dissipative deformation mechanisms in steels under cyclic loading. International Journal of Plasticity 32–33: 106–120.

Papakyriacou M, Mayer H, Pypen C, Plenk H, Stanzl-Tschegg S (2001) Influence of loading frequency on high cycle fatigue properties of b.c.c. and h.c.p. metals. Materials Science and Engineering: A 308(1): 143–152.

Rafi HK, Starr TL, Stucker BE (2013) A comparison of the tensile, fatigue, and fracture behavior of Ti–6Al–4V and 15-5 PH stainless steel parts made by selective laser melting. Int J Adv Manuf Technol 69(5–8): 1299–1309.

Rickenbacher L, Spierings A, Wegener K (2013) An integrated cost-model for selective laser melting (SLM). Rapid Prototyping Journal 19(3): 208–214.

Spears T, Gold S (2016) In-process sensing in selective laser melting (SLM) additive manufacturing. Integrating Materials and Manufacturing Innovation 5.

Terris T de, Andreau O, Peyre P, Adamski F, Koutiri I, Gorny C, Dupuy C (2019) Optimization and comparison of porosity rate measurement methods of Selective Laser Melted metallic parts. Additive Manufacturing 28: 802–813.

Thijs L, Verhaeghe F, Craeghs T, Humbeeck JV, Kruth J-P (2010) A study of the microstructural evolution during selective laser melting of Ti–6Al–4V. Acta Materialia 58(9): 3303–3312.

Vrancken B, Thijs L, Kruth J-P, Van Humbeeck J (2012) Heat treatment of Ti6Al4V produced by Selective Laser Melting: Microstructure and mechanical properties. Journal of Alloys and Compounds 541: 177–185.

Wycisk E, Emmelmann C, Siddique S, Walther F (2013) High Cycle Fatigue (HCF) Performance of Ti-6Al-4V Alloy Processed by Selective Laser Melting. Advanced Materials Research 816–817: 134–139.

Wycisk E, Siddique S, Herzog D, Walther F, Emmelmann C (2015) Fatigue Performance of Laser Additive Manufactured Ti–6Al–4V in Very High Cycle Fatigue Regime up to 109 Cycles. Front Mater 2.

Wycisk E, Solbach A, Siddique S, Herzog D, Walther F, Emmelmann C (2014) Effects of Defects in Laser Additive Manufactured Ti-6Al-4V on Fatigue Properties. Physics Procedia 56: 371–378.

Yang J, Yu H, Yin J, Gao M, Wang Z, Zeng X (2016) Formation and control of martensite in Ti-6Al-4V alloy produced by selective laser melting. Materials & Design 108: 308–318.